THE EFFECTS OF PRE-BOND CONTAMINATION WITH DE-ICING FLUID ON THE MODE-I AND MODE-II FRACTURE TOUGHNESS OF COMPOSITE BONDED JOINTS

E. MOUTSOMPEGKA

Department of Mechanical Engineering & Aeronautics, University of Patras
Laboratory of Technology & Strength of Materials,
Patras 26500, Greece
mucobega@mech.upatras.gr

P. POLYDOROPOULOU

Department of Mechanical Engineering & Aeronautics, University of Patras
Laboratory of Technology & Strength of Materials,
Patras 26500, Greece
ppolydor@mech.upatras.gr

K. I. TSERPES*

Department of Mechanical Engineering & Aeronautics, University of Patras
Laboratory of Technology & Strength of Materials,
Patras 26500, Greece
kitserpes@upatras.gr

C. TORNOW

Fraunhofer Institute for Manufacturing Technologies and Advanced Materials (IFAM)
Wiener Str. 12 28359 Bremen, Germany
christian.tornow@ifam.fraunhofer.de

M. SCHLAG

Fraunhofer Institute for Manufacturing Technologies and Advanced Materials (IFAM)
Wiener Str. 12 28359 Bremen, Germany
mareike.schlag@ifam.fraunhofer.de

K. BRUNE

Fraunhofer Institute for Manufacturing Technologies and Advanced Materials (IFAM)
Wiener Str. 12 28359 Bremen, Germany
kai.brune@ifam.fraunhofer.de

B. MAYER

Fraunhofer Institute for Manufacturing Technologies and Advanced Materials (IFAM)
Wiener Str. 12 28359 Bremen, German
bernd.mayer@ifam.fraunhofer.de

S. PANTELAKIS

Department of Mechanical Engineering & Aeronautics, University of Patras
Laboratory of Technology & Strength of Materials,
Patras 26500, Greece
pantelak@mech.upatras.gr

Abstract

Damaged carbon fibre reinforced plastic (CFRP) aircraft parts may have been subjected during service to a range of hostile chemicals before being repaired by adhesively bonded patches. One chemical that could contaminate aircraft parts is the de-icing fluid used to maximize the runway friction during all plane movements at airports in winter. The scope of the present work is to experimentally investigate the effect of pre-bond contamination with de-icing fluid on integrity of CFRP bonded joints by conducting mode-I and mode-II fracture toughness tests on both reference and contaminated specimens. The de-icer used to contaminate the surface of one adherent was diluted with demineralized water to obtain solutions with the following concentrations in vol%: 2% (low level contamination, DI-1), 7% (medium level contamination, DI-2) and 10% de-icer (high level contamination, DI-3). Then, it was applied on the surfaces by dip coating and dried in the oven for 2h at 40°C. Afterwards, acclimatization at RT was allowed for at least 24h. The dip coating results were controlled by XPS measurements. Since the de-icer contains potassium formiate, the potassium content on the surface was taken as a measure for the degree of de-icer contamination. XPS-results showed mean values and standard deviations from two dip coated samples with three measuring positions each: DI-1: 6.4 (±1.8) at% K, DI-2: 10.9 (±2.3) at% K, DI-2: 12.0 (±1.4) at% K. The experimental results revealed a detrimental effect of de-icing fluid on the integrity of the joints. Specifically, for DI-1 a reduction of 30% and 56% is observed for G_{IC} and $G_{IIC,}$ respectively, with regard to the

reference values (non-contaminated joints), for DI-2 the corresponding values are 37% and 62% and for DI-3 it is 56% and 83%. Regarding the fracture surfaces, it was observed that with increasing the contamination level the presence of light-fiber-tear failure mode increases, which indicates that the de-icing fluid has a deleterious impact on the composite material.

Keywords CFRP adhesive bonds; pre-bond contamination; de-icing fluid; fracture toughness.

1. Introduction

The use of adhesive bonding has been continually increasing in aircraft structures both for assembling structural parts and applying composite patch repairs due to the numerous advantages they provide over conventional techniques for fastening materials (Markatos *et al.*, 2014; da Silva *et al.*, 2011; de Moura *et al.*, 2008; Ebnesajjad, 2008; Ashcroft and Crocombe, 2008; Charalambides *et al.*, 1998) such as more uniform stress distribution in the joint, ability to join dissimilar materials, better fatigue properties, attractive strength to weight ratio, etc.

However, the application of adhesive bonding technology is limited to joining and patch-repairing of structures that are not load-critical. Amongst the disadvantages associated with adhesive bonding (Markatos *et al.*, 2014; da Silva *et al.*, 2011; de Moura *et al.*, 2008; Ebnesajjad, 2008; Ashcroft and Crocombe, 2008; Charalambides *et al.*, 1998), a factor which hinders the wider application of adhesive joints is the sensitivity of the bondline integrity to the environmental factors (Markatos *et al.*, 2014; da Silva *et al.*, 2011; de Moura *et al.*, 2008; Charalambides *et al.*, 1998; Tserpes *et al.*, 2014) adhesively bonded joints are exposed to during service. Runway de-icing fluid is one of the most commonly encountered fluids that adhesive bonded composite structures may be exposed to. Runway de-icers are essential to safe airport operations and are used to maximize the runway friction during all plane movements at airports in winter. Generally, airfield pavement de-icing products (PDPs) traditionally consisting of urea or glycols have become less popular owing to their adverse environmental impacts (Shan Yong, 2001; Shi, 2008). New PDPs have emerged as alternatives that often contain potassium acetate (KAc), sodium acetate (NaSc), sodium formate (NaF), or potassium formate (KF) as the freezing point depressant (Shi, 2008).

In contrast with other environmental factors, such as moisture or temperature, no research has been published on the effect of runway de-icing fluid on the adhesive composite bonds, while the publications on the effect of the de-icing fluid on aircraft composite parts are mainly limited to field reports from airports (Shan Yong, 2001; Shi, 2008; Arriaga, 2008; Myhra, 2015). A growing body of field evidence from airline operators indicated that KAc and KF may cause accelerated structural degradation of carbon-carbon (C/C) composite aircraft brakes as a result of the catalytic oxidation by the potassium cation, which may result in reduced brake life and introduce the possibility of brake failure (Shi, 2008). The low melting temperatures of K salts and their decomposition products -all below 327^{o}C- allow them to migrate easily on the carbon surface and form good interfacial contact with it, facilitating oxygen transfer (Shi, 2008).

In the present work, the effect of pre-bond de-icing fluid contamination on mode-I and mode-II fracture toughness of CFRP bonded joints is quantitatively studied by considering the exposure of the CFRP adherents in three different de-icing fluid concentrations.

2. Pre-bond contamination of CFRP adherents

2.1 Materials

Hexcel® M21E is the material used for the preparation of test coupons. HexPly M21E/IMA, developed from Hexcel®'s M21 third generation thermosetting epoxy resin system, is using an intermediate modulus fibre balancing superior strength and stiffness which was developed specifically for Airbus. The resin matrix was developed to ensure optimal translation of the carbon fibre properties whilst delivering outstanding fracture resistance. The sample plates were produced by Aernnova Composites using liquid water based silicon-containing release agent Frekote® C-600, in order to obtain smooth surfaces.

Regarding the structural layout, CFRP monolithic structures were manufactured according to Airbus AIPS 03-02-019 standard for CFRP ("Manufacture of monolithic parts with thermoset prepreg materials"). The adherents consisted of 8 unidirectional plies and their layup sequence was [0, 0, 45, -45, -45, 45, 0, 0] according to AITM 1-0053 (Airbus S.A.S, 2006) standard. A release film of 25 mm length was inserted at one end of the sample prior to bonding to obtain an initial delamination for fracture toughness tests. Film adhesive FM® 300-2

from Cytec (0.2 mm thickness) was used for the adhesive bonding instead of paste, in order to standardize its thickness and increase reliability of results.

2.2 Samples Preparation

2.2.1 Adherents preparation

To prepare the clean reference samples from the delivered plates the following steps were performed and each step was monitored by X-ray photoelectron spectroscopy (XPS) analyses (Fig. 1):

(1) Pre-cleaning of the plates with Isopropanol (IPA)-soaked tissues to remove part of the release agent and any other soluble contaminations, e.g. fingerprints, remained from the manufacturing process. XPS measurements performed on the "as delivered" plates on three different positions showed an inhomogeneous distribution of Si-containing release agent on the CFRP surface (Table I). The XPS results on the cleaned plates showed that pre-cleaning with IPA is effective in a sense that the amount of release agent on the CFRP surface can be reduced by it to a value of 0.5-1.4 at%. This is an amount which can easily be removed by the subsequent grinding step.

(2) Slight grinding of the surfaces to remove residual release agent which had penetrated or was incorporated into the topmost resin layers and afterwards wiping with demineralized H_2O and IPA to remove the dust from a grinding and residual silicone. The new XPS measurements conducted showed a small amount of silicone remained on the surface (Table I).

(3) A second slight grinding step, followed by wiping off the dust with demineralized water and IPA. On these samples, XPS measurements showed a very clean surface (Table I).

After the cleaning steps, the sample plates were wiped with methyl ethyl ketone (MEK)-soaked tissues prior to contamination and adhesive bonding.

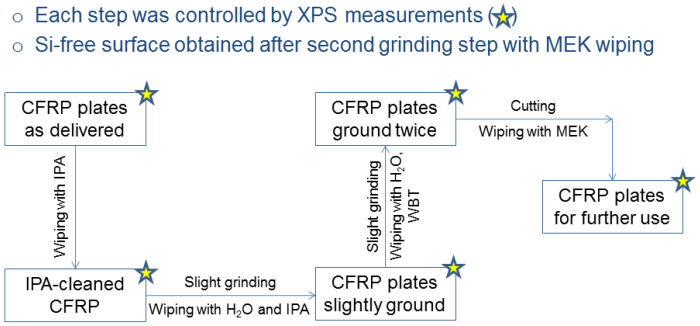

Fig. 1. Scheme for cleaning of as-received CFRP plates.

Table I. XPS results for the CFRP sample plates at the cleaning steps.

CFRP plates	Si (at%)
CFRP "as delivered" sample plates	5.3 ± 1.3
CFRP sample plates after IPA cleaning	0.9 ± 0.5
CFRP sample plates after IPA cleaning and slight grinding	0.3 ± 0.2
CFRP sample plates after IPA cleaning and two slight grinding steps with cleaning in between	0.1 ± 0.04

2.2.2 Adherents contamination and bonding

The de-icer used was SAFEWAY® KF from CLARIANT. It was diluted with demineralized water to obtain solutions with the following concentrations in vol%: low level 2% (DI-1), medium level 7% (DI-1) and high level of contamination 10% (DI-3). It was applied on the surfaces by dip coating (aqueous solution) and then dried in the oven for 2h at 40°C. Then acclimatization at room temperature was allowed for at least 24h. The dip coating results were controlled by XPS measurements. Since the de-icer contains potassium formiate, the potassium content on the surface is taken as a measure for the degree of de-icer contamination. XPS-results are shown in Table II.

For the bonding of the CFRP plates, the adhesive was cured in an autoclave cycle in accordance with the material data sheet specifications. Finally, the sample plates were cut to the final specimen dimensions specified by the standards of the mechanical tests. Cutting was performed dry (diamond cutting) to prevent any contamination of the cleaned surfaces. After cutting, the surfaces were cleaned again with IPA soaked tissues.

Table II: XPS-results for CFRP samples with different de-icer dip coating concentrations.

Scenario	K (at%)
DI-1	6.4 ± 1.8
DI-2	10.9 ± 2.3
DI-3	12.0 ±1.4

3. Experimental

Mode-I and mode-II tests were conducted to characterize the fracture toughness in terms of energy release rate G and assess the effect of runway de-icing fluid on the CFRP bonded joints.

3.1 Mode-I fracture toughness test

The Airbus specification AITM 1-0053 (Airbus S.A.S, 2006) defines a method to determine the mode-I fracture toughness energy G_{IC} of carbon fibre composite bonded joints. The double cantilever beam (DCB) specimen is used, which consists of rectangular adherents bonded along their length incorporating a region of non-adhesive release film at one end for the introduction of the initial crack in the bondline (Fig. 2). Loading was applied to the DCB specimen via metallic piano hinges bonded to the adherents at one end. In order to avoid any influence of the incorporated release film, the specimen was preloaded until an initial crack length of 10 to 15 mm was achieved. The pre-cracked specimen was then loaded continuously by opening forces until total propagated crack length of 100 mm was achieved. After that, the test stopped and the specimen was unloaded.

During the crack propagation the load and crosshead displacement of the test machine were recorded continuously. A traveling microscope was used to facilitate the visual measurement of the crack length. The DCB specimen is nominally of 250 mm length, 25 mm width and 3 mm thickness, while the release film is 25 mm long. Six specimens per scenario were tested under a tensile loading using a Tinius Olsen H5K-S universal testing machine with a load cell of 5 kN at room temperature (25^{o}C) under displacement control. In order to avoid an increase in the amount of unstable crack propagation at high crosshead rates (Davies and Benzeggagh, 1989), the rate was kept constant at 5 mm/min. Fig. 3 illustrates a specimen mounted on the tensile testing machine during mode-I test.

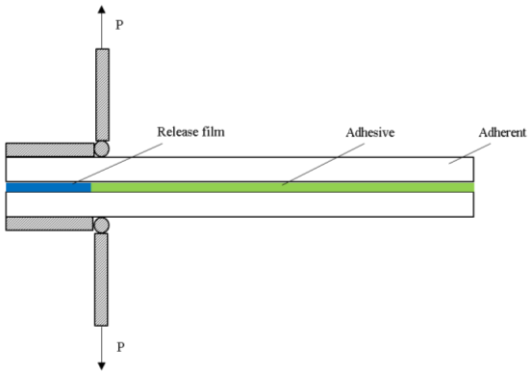

Fig. 2. Schematic representation of the DCB specimen.

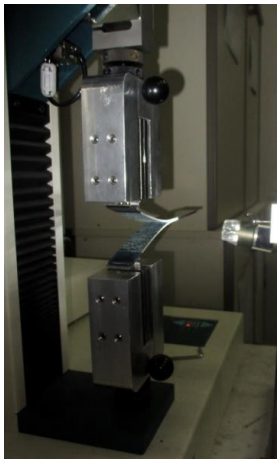

Fig. 3. DCB specimen under mode-I loading.

The area method was applied to interpret the data recorded during mode-I tests. The crack extension is related directly to the area enclosed between the loading and unloading curves as shown in Fig. 4. The mode-I fracture toughness energy G_{IC} is defined as follows (Airbus S.A.S, 2006):

$$G_{IC}=\frac{A}{a\times w}\times 10^{6} \quad (J/m^2) \qquad (1)$$

where:

A	is the energy to achieve the total propagated crack length (integration of the area of the load-crosshead displacement diagram)	(J)
a	is the propagated crack length ($a=a_{final}-a_{initial}$)	(mm)
w	is the width of the specimen	(mm)

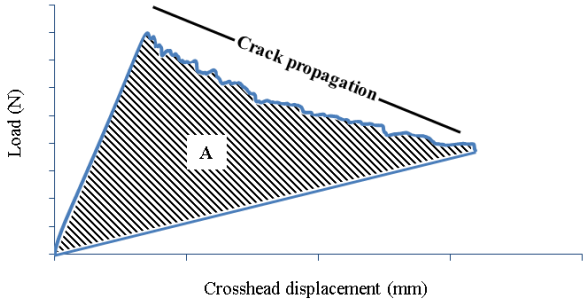

Fig. 4. Mode-I load-displacement diagram.

The most popular means of investigating delamination mechanisms in mode-I it the examination of fracture surfaces (Davies and Benzeggagh, 1989). So, after the tests, the failure surfaces were examined in order to accurately assess the causes of adhesive bond failures (Markatos *et al.*, 2014; Tserpes *et al.*, 2014; Davis and Bond, 1999). There are three basic ways in which an adhesive bonded joint may fail: cohesive, adhesive and fracture in the adherent. Usually, a mixed failure occurs when symptoms of several of the previous failures are observed simultaneously. Failure of the adherent outside the joint is achievable for well-designed and fabricated adhesive bonds in moderately thin adherent materials. This condition is desirable as it enables the full structural performance of the adherents to be utilized (Davis and Bond, 1999). Cohesive bond failure results in fracture of the adhesive and is characterized by the clear presence of adhesive material on both laminates of the bonded specimen. Pure cohesive failure is highly desired as it denotes an ideally designed and manufactured bonded joint (Markatos *et al.*, 2014). Adhesive failure occurs along the interface between the adhesive layer and the laminate and is characterized by the absence of adhesive on one of the adherent surfaces. Adhesive failure is an indication of a weak bond and is unacceptable in aerospace industry.

3.2 Mode-II fracture toughness test

Up to now, there is no standardized test to measure the fracture toughness energy of bonded joints under pure mode-II loading (de Moura, 2008; de Moura *et al.*, 2009; Pearson *et al.*, 2012). Although fracture characterization of bonded joints under pure mode-I has been extensively studied and standardized, mode-II is still not well addressed owing to some practical aspects inherent to the most popular tests: the End Notched Flexure (ENF), the End Loaded Split (ELS) and the Four-Point End Notched Flexure (4ENF). The ELS test involves a clamp which is a source of variability and increases the complexity of data reduction (de Moura, 2008; de Moura *et al*., 2009). On the other hand, the 4ENF test requires a complex setup and presents some problems related to large friction effects reduction (de Moura, 2008; de Moura *et al*., 2009). As a consequence, the ENF specimen has emerged as the most convenient mode-II fracture toughness specimen. The specimen is easy to manufacture, the test fixture is simple and the data-reduction methodology straightforward (Carlsson and Gillespie, 1989).

Fig. 5 illustrates a schematic representation of the ENF test. A pre-cracked specimen is loaded in a three point bend fixture until the crack propagation onset. The pre-crack is embedded through-width at the end of the specimen to accommodate the sliding deformation of the adherents that result from the flexural loading (Carlsson and Gillespie, 1989). In order to provide crack growth stability the initial crack length was considered to be equal to 70% of L/2 (Ebnesajjad, 2008; Pearson *et al.*, 2012). The load applied to the specimen and the cross head displacements of the test machine were recorded continuously during the test.

Mode-II tests were conducted according to the AITM 1-0006 (Airbus S.A.S, 1994) standard at room temperature under a constant displacement rate of 1 mm/min using an MTS universal testing machine with a load capacity of 100 kN (Fig. 6).The test specimens were cut from the residual part of G_{IC} specimens so that a pre-crack of 35 mm was achieved. Three specimens were tested for each condition. In order to facilitate the optical observation of the crack tip and the detection of the crack propagation onset, a digital microscope was used and a thin layer of white ink was applied to the longitudinal side faces of the specimen.

To calculate G_{IIC} fracture toughness energy the following formula was used (Airbus S.A.S, 1994):

$$G_{IIC}=\frac{9\times P\times a^2\times d\times 1000}{2\times w\times\left(1/4\times L^3+3\times a^3\right)} \quad (J/m^2) \quad (2)$$

where:

d	is the crosshead displacement at crack propagation onset	(mm)
P	is the critical load to start the crack propagation	(P)
a	is the initial crack length	(mm)
w	is the width of the specimen	(mm)
L	is the span length	(mm)

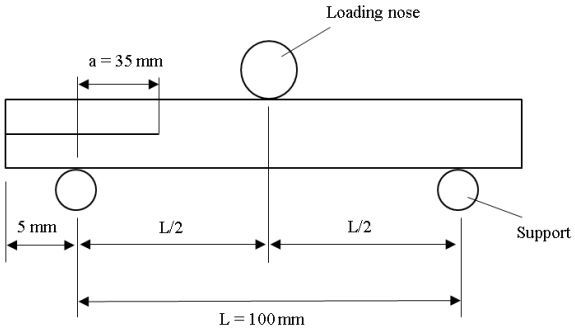

Fig. 5. Schematic representation of the ENF tests.

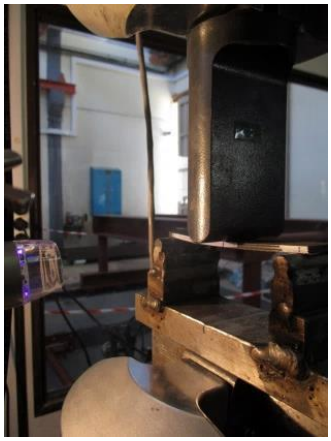
Fig. 6. Mode-II experimental setup.

4. Results and Discussion

4.1 Mode-I Fracture Toughness Test Results

4.1.1 Effect of de-icing fluid

The experimental load-displacement curves of the mode-I tests of the different de-icing fluid concentration categories, including the reference one, are plotted in Fig. 7. It is observed that all specimens exhibited an unstable crack growth. The computed G_{IC} values of the specimens are listed in Table III, while the histogram of Fig. 8 compares the average G_{IC} values at crack propagation of the three sets of de-icing fluid contaminated samples with that of the reference samples. As expected, the reference category specimens exhibited the highest values. The results indicate a negative effect of the de-icing fluid as G_{IC} is reduced for all three contaminated sample categories. Specifically, for DI-1 the average G_{IC} values show an almost 30% reduction compared to the reference category, for DI-2 the average G_{IC} is reduced further to 37%, while for DI-3 the fracture toughness of the joints degrades significantly by 56% designating the detrimental effect of the de-icing fluid on the bond performance. The rather big scatter of the G_{IC} values of the specimens tested for the same category denotes mainly the complexity of the adhesion mechanisms as well as the non-uniform affects in the contaminants (Markatos *et al.*, 2014; Tserpes *et al.*, 2014). It could also be attributed to the crack propagation manner, as the crack propagated in a non-uniform unstable manner for the specimens of each category and the failure mode varied requiring different amounts of energy for the crack to propagate as it will be discussed in section 4.1.2.

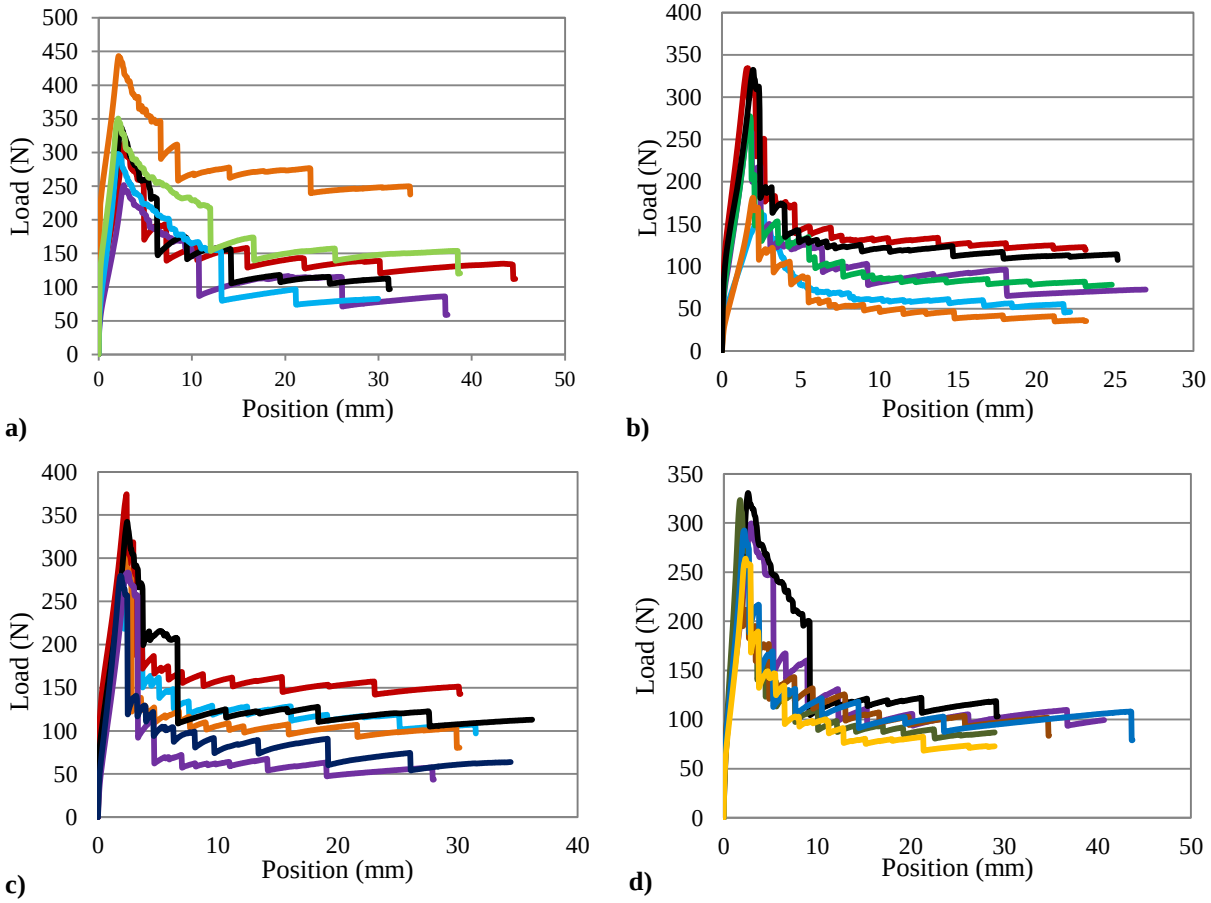

Fig. 7. Experimental mode-I load-displacement curves of a) reference specimens, b) DI-1 specimens, c) DI-2 specimens and d) DI-3 specimens.

Table III. Experimental G_{IC} values.

Scenario	G_{IC} (J/m^2)
REF	1338.48 ± 350.45
DI-1	926.50 ± 170.66
DI-2	842.90 ± 204.74
DI-3	588.18 ± 164.47

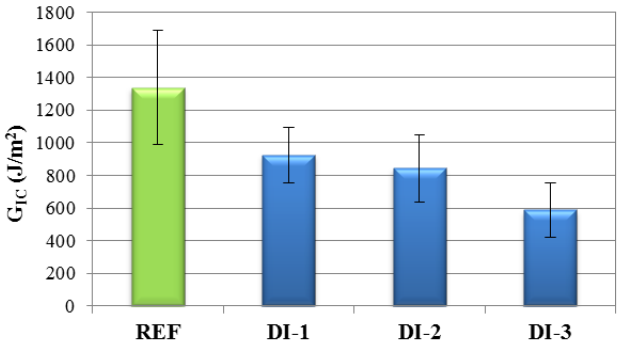

Fig. 8. Average G_{IC} values comparison.

4.1.2 Failure modes characterization

The classification, identification and characterization of the failure mode of the CFRP bonded joints were conducted according to ASTM D5573 (ASTM International, 2005) standard. Besides the three basic failure modes described previously, the ASTM D5573 standard defines a number of sub-modes such as fiber-tear failure

in which failure occurs exclusively within the fiber-reinforced polymer matrix resulting in the appearance of fibers on both ruptured surfaces, and light-fiber-tear where failure occurs within the adherent, near the surface, characterized by a thin layer of the matrix on the adhesive, with few or no fibers transferred from the substrate to the adhesive.

Firstly, for the reference samples mixed-mode failure was observed with the dominant failure being the light-fiber-tear failure at a percentage of 50%, while the cohesive failure was observed at 35% of the surface area and the adhesive failure at 15% (Table IV). Representative failure surfaces are shown in Fig. 9. The adhesive failure results show a large scatter which is attributed to the fact that not all six specimens presented homogeneous failure as three samples presented adhesive failure at a percentage less than 4%. The phenomenon of the non-uniform failure mode amongst samples of the same set is present in the contaminated samples sets also, revealing the complexity of crack propagation in adhesive bonds and mode-I fracture toughness tests.

For the DI-1 scenario the cohesive failure was reduced to 11.71% while larger surface failed adhesively (26%) indicating the reduction in the bond strength. Light-fiber-tear failure remained the dominant failure with an increasing value of 63%. Finally, for the DI-3 set, adhesive and cohesive failure modes were reduced drastically to 0.25% and 5 % respectively, while 90% of the surface area failed in light-fiber-tear mode. It is worth mentioning that one of the specimens presented fiber tear failure. The increase of the light-fiber tear and fiber-tear failure as a result of the increased de-icing fluid contamination indicates that de-icing fluid has a deleterious impact mainly on the CFRP adherents.

Table IV: Percentages of failure modes.

Scenario	Adhesive failure	Cohesive failure	Light-fiber-tear failure	Fiber-tear failure
REF	14.83% (±15.79)	35.33% (±8.82)	49.83% (±11.92)	0.00%
DI-1	25.73% (±24.77)	11.71% (±8.51)	62.57% (±19.56)	0.00%
DI-2	12.83% (±16.05)	12.62% (±2.81)	74.55% (±18.38)	0.00%
DI-3	0.25% (±0.42)	5.33% (±1.83)	89.62% (±12.35)	4.80% (±11.76)

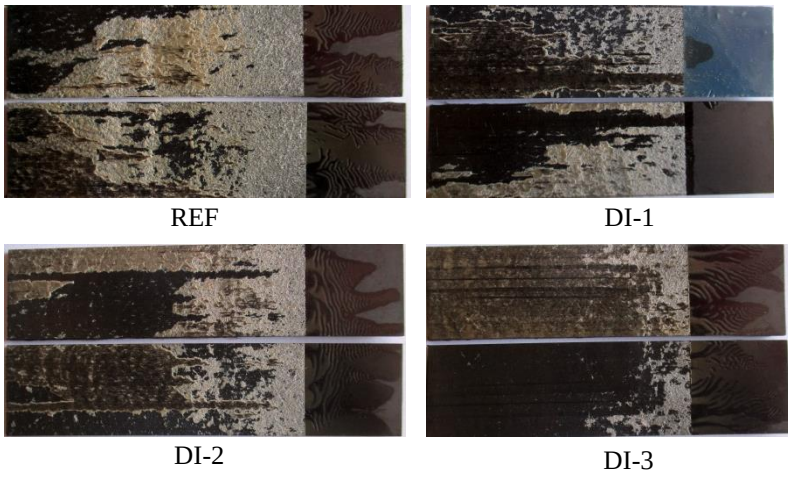

Fig. 9. The failure modes of the de-icing fluid contamination scenarios.

4.2 Mode-II Fracture Toughness Test Results

The experimental load-displacement curves of the ENF specimens are presented in Fig. 10. The curves show an initial linear behavior of the specimens followed by the region where matrix cracking started to accumulate at the adherents until macroscale failure of the outer layers of the adherents as a result of compression. Usually, the load increases until the crack initiation process is completed and after that the crack tip starts propagating and the load continuously drops. However, at the present study, the crack propagation onset was observed long before the load drop point, which made the precise crack propagation onset determination more difficult. This is probably due to the small adhesive thickness compared to the laminate as the adhesive has a slight contribution to the bond's rigidity resulting in no visible reduction of the bending stiffness of the adhesive bond when crack propagation onset in the adhesive or interface occurs (Floros *et al.,* 2015). When the crack reaches the ENF

specimen's middle, at the time crack approaches the loading cylinder, the load starts to increase due to the compression near the crack tip which obstructs propagation because of friction effects (de Moura *et al.*, 2009; Pearson *et al.*, 2012).

The G_{IIC} values of the specimen, listed in Table V, were computed using Equation (2). As in mode-I tests, the impact of runway de-icing fluid on the mode-II fracture toughness is detrimental. The increase of the de-icing fluid concentration causes a further G_{IIC} reduction (Fig. 11). Specifically, for DI-1 a reduction of 56% is observed with regard to the reference values, for DI-2 the corresponding value is 62 %, while for DI-3 the reduction reaches 80%.

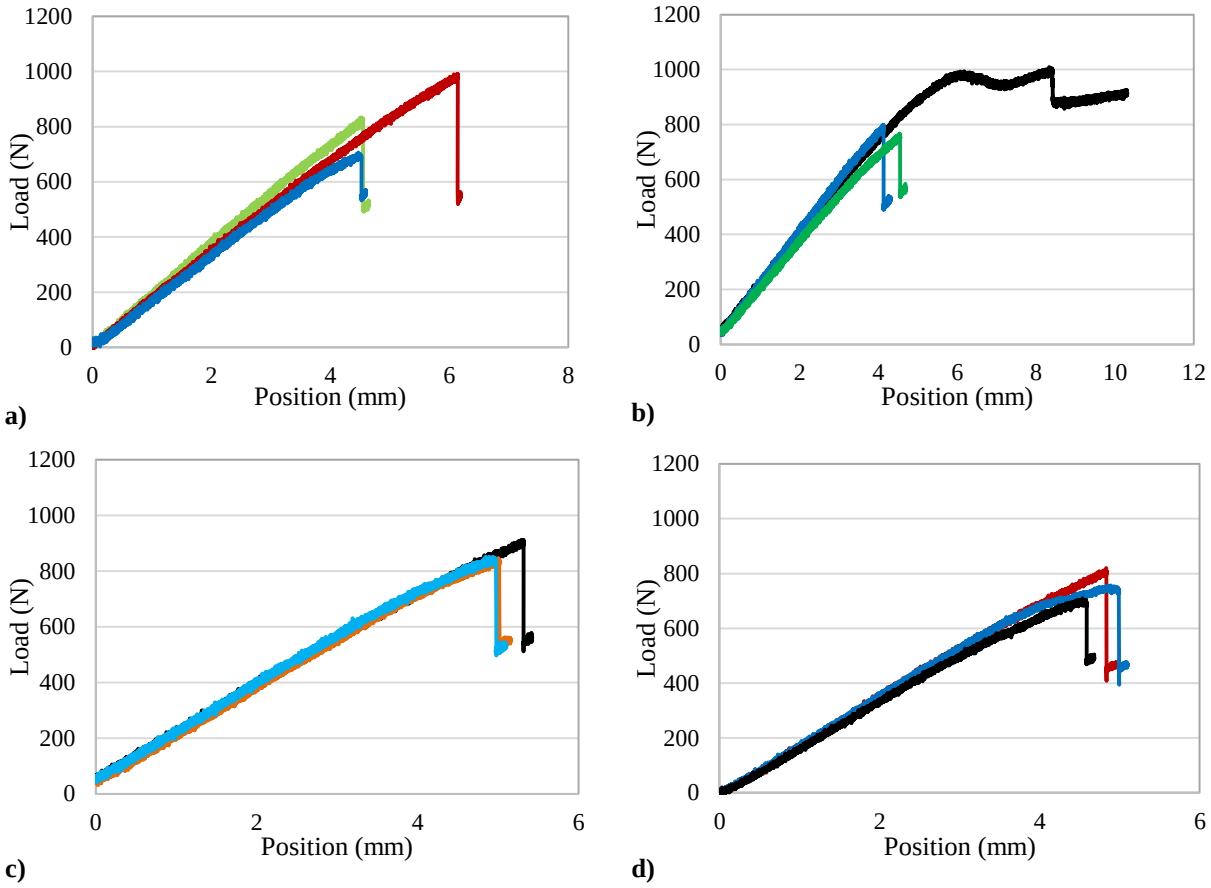

Fig. 10. Experimental mode-II load-displacement curves of a) reference specimens, b) DI-1 specimens, c) DI-2 specimens and d) DI-3 specimens.

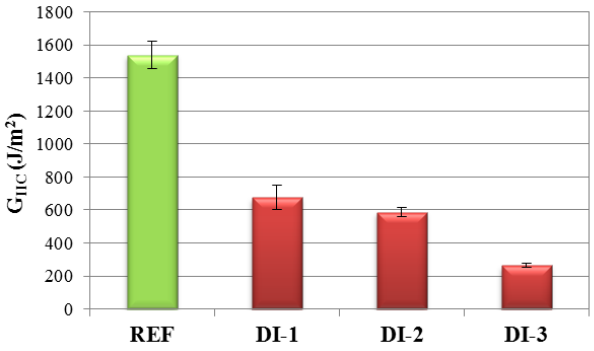

Fig. 11. Average G_{IIC} values comparison.

Table V: Experimental G_{IIC} values.

Scenario	G_{IIC} (J/m^2)
REF	1539.25 ± 82.08
DI-1	676.29 ± 76.05
DI-2	587.06 ± 27.84
DI-3	264.47 ± 14.61

5. Conclusions

In the present work, the effect of pre-bond contamination with runway de-icing fluid on the mode-I and mode-II fracture toughness of CFRP composite bonded joints was experimentally studied. This scenario is possible to appear in the implementation of a composite patch repair in a damaged composite structural part as de-icing fluid can be swirled from the runway to outer parts of the aircraft. Three different levels of de-icing fluid contamination, namely low level 2% (DI-1), medium level 7% (DI-1) and high level of contamination 10% (DI-3) were used. From the experimental results the following conclusions can be drawn:

- The pre-bond contamination with de-icing fluid significantly degraded the performance of the joints by decreasing both the mode-I and mode-II fracture toughness energy.
- The mode-I and mode-II fracture toughness decreased further with increasing de-icing fluid concentration.
- The mode-I experimental results show a considerable scatter which is common for fracture toughness tests and denotes mainly the complexity of the adhesion mechanisms as well as the non-uniform affects in the contaminants. Also, the non-uniform unstable manner of crack propagation that specimens exhibited enhanced the big scatter.
- Joints failed under mixed-mode failure with the light-fiber tear failure being the dominant to all sample sets.
- With the increase of the contaminant concentration, the light-fiber tear failure mode increased in percentage of the failure surfaces which indicates that de-icing fluid has a deleterious impact mainly on the CFRP adherents.
- Under mode-II load conditions, the crack initiation occurred before the maximum load and thus it did not change the slope of the force-displacement curve due to the relatively low adhesive thickness compared to the adherents' thickness.
- Mode-II experimental results showed a small scatter compared to the mode-I results.

Acknowledgements

The research leading to these results has received funding from the European Union's Horizon 2020 research and innovation program under grant agreement n^o 636494 (Project COMBONDT: Quality Assurance Concepts for Adhesive Bonding of Aircraft Composite Structures by Extended NDT).

References

D.N. Markatos, K.I. Tserpes, E. Rau, K. Brune, Sp. Pantelakis, Degradation of mode-I fracture toughness of CFRP bonded joints due to release agent and moisture pre-bond contamination, Journal of Adhesion 90 (2), pp. 156-173 (2014)

L.F.M da Silva, A. Öchsner, R.D. Adams. 2011. Introduction to adhesive bonding technology. In: L.F.M da Silva, A. Öchsner, R.D. Adams (Eds). Handbook of Adhesion Technology (Vol 2). Springer- Verlag Berlin Heidelberg, pp 2-3

M.F.S.F de Moura. 2008. Progressive damage modelling. In: L.F.M da Silva and A. Öchsner. Eds. Modeling of adhesively bonded joints. Springer- Verlag Berlin Heidelberg, pp 155-156,166-171

S. Ebnesajjad, Adhesives technology Handbook, 2nd Edition, William Andrew Inc, 2008.

I.A. Ashcroft and A.D. Crocombe. 2008. Modelling the fatigue in adhesively bonded joints. In: L.F.M da Silva and A. Öchsner. Eds. Modeling of adhesively bonded joints. Springer-Verlag Berlin Heidelberg, pp 184

M.N. Charalambides, R. Hardouin, A.J. Kinloch, F.L. Matthews, Adhesively-bonded repairs to fibre-composite materials I. Experimental, Composites Part A: Applied Science and Manufacturing, Volume 29, Issue 11, November 1998, Pages 1371–1381

K.I. Tserpes, D.N. Markatos, K. Brune, M. Hoffmann, E. Rau, Sp. Pantelakis, A detailed experimental study of the effects of pre-bond contamination with a hydraulic fluid, thermal degradation, and poor curing on fracture toughness of composite-bonded joints, Journal of Adhesion Science and Technology 28 (18), pp. 1865-1880 (2014)

J. Shan Yong, Evaluation of the environmental impact and alternative technologies of deicing/anti-icing operations at airports, Master of Engineering in Civil and Environmental Engineering, Massachusetts Institute of Technology, 2001
Xianming Shi, Airport Cooperative Research Program Synthesis 6, Impact of airport pavement deicing products on aircraft and airfield infrastructure, Transportation research board, Washington, D.C, 2008
Michael Arriaga, Runway de-icing material effects on aircraft carbon brakes. G-12F Aircraft ground deicing fluids subcommittee, Catalytic oxidation working group, SAE International, Colorado, 2008
T. Myhra, Deicing and anti-icing decisions for runways and ramps, Washington Airport Management Association (WAMA) Conference 2015
AITM 1-0053 (2006), AITM, Airbus Test Method, Carbon Fibre Reinforced Plastics, Determination of fracture toughness energy of bonded joints, Mode I, Airbus S.A.S, France, 2006
P. Davies, M.L. Benzeggagh.1989. Interlaminar mode-I fracture testing. In: K. Friedrich (Ed). Application of Fracture Mechanics to Composite Materials. Elsevier Science Publishers B.V., pp 81-112
M.F.S.F. de Moura, R.D.S.G Campilho, J.P.M Goncalves, Pure mode II fracture characterization of composite bonded joints, International Journal of Solids and Structures 46 (2009) 1589-1595
R. A. Pearson, B.R.K. Blackman, R.D.S.G. Campilho, M. F.S.F. de Moura, N.M.M. Dourado, R.D. Adams, D.A. Dillard, J.H.L. Pang, P. Davies, A. Ameli, S. Azari, M. Papini, J.K. Spelt, E. Nicoli, H.K. Singh, C.E. Frazier, S. Giannis, K.B. Armstrong, N. Murphy, L.F. Kawashita.2012. Quasi-Static Fracture Tests. In: L.F.M da Silva, D.A. Dillard, B. Blackman, R.D. Adams (Eds). Testing Adhesive Joints: Best Practices. Wiley-VCH Verlag & Co. KGaA, pp 163-191
L.A. Carlsson, J.W Gillespie Jr.1989. Mode-II interlaminar fracture of composites. In: K. Friedrich (Ed). Application of Fracture Mechanics to Composite Materials. Elsevier Science Publishers B.V., pp 113-122
AITM 1-0006 (1994), AITM, Airbus Industry Test Method, Carbon Fibre Reinforced Plastics, Determination of interlaminar fracture toughness energy, Mode II, Airbus S.A.S, France, 1994
I. Floros, K.I. Tserpes, T. Lobel, Mode-I, mode-II and mixed-mode I+II fracture behavior of composite bonded joints: Experimental characterization and numerical simulation, Composites Part B: Engineering (78), pp.459-468, (2015)
M.J. Davis, D.A. Bond (1999), The importance of failure mode identification in adhesive bonded aircraft structures and repairs, Paper presented at: International Conference on Composite Materials 12 (ICCM-12), France, ICCM-12 Online Proceedings
M.J. Davis, A. McGregor (2010), Assessing adhesive bond failures: Mixed-mode bond failure explained, Paper presented at ISASI Australian Safety Seminar, Canberra
ASTM D5573-99(2005), Standard Practice for Classifying Failure Modes in Fiber-Reinforced-Plastic (FRP) Joints, ASTM International, West Conshohocken, PA, 2005, www.astm.org